2023-04-15

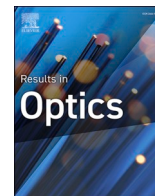# Highly sensitive biosensor based on a microstructured photonic crystal fibre for alcohol sensing

Ang, Chuan

Provided with love from The Nelson Mandela African Institution of Science and Technology

Highly sensitive biosensor based on a microstructured photonic crystal fibre for alcohol sensing

Chuan Shi Ang [a], Abdul Mu'iz Maidi [a], Shubi Kaijage [b], Feroza Begum [a,*]

[a] *Faculty of Integrated Technologies, Universiti Brunei Darussalam, Jalan Tungku Link, Gadong, Bandar Seri Begawan BE1410, Brunei*
[b] *School of Computational and Communication Science and Engineering, Nelson Mandela African Institution of Science and Technology, Arusha 23311, Tanzania*

ARTICLE INFO

ABSTRACT

A microstructure alcohol biosensor has been proposed to operate in the wavelength range of 0.8 to 2.0 μm for the sensing of propanol, butanol, and pentanol, unveiling impressive results of relative sensitivity and confinement loss. The results are achieved by implementing closely arranged cladding air holes of 3 rings with a single elliptical core hole for analyte infiltration. Performance evaluation of the sensor was conducted using COMSOL Multiphysics software and yields relative sensitivity of 96.75%, 89.60%, and 82.02% for propanol, butanol, and pentanol, respectively, and confinement losses of 5.49×10^{-12} dB/m for propanol, 1.98×10^{-12} dB/m for butanol, and 9.36×10^{-13} dB/m for pentanol. Other optical parameters have also been analysed that recorded effective refractive index, high power fraction, low birefringence, small effective area, and large nonlinear coefficients. The proposed biosensor is eligible for practical application in alcohol sensing with these results. Moreover, this proposed biosensor is suitable as a supercontinuum source in optical communication systems because of the high nonlinear coefficients.

1. Introduction

Optical fibres have profoundly progressed since the introduction of lasers in the 90s (Kadhum Hisham, 2018). With the advancement of technologies, optical fibres have been developed to improve the quality of life and further enhance the standard of living through the different fields of communication, illumination, optical imaging, sensors and many more (Yang et al., 2019). Photonic Crystal Fibres (PCFs) are the type of optical fibre constructed of microscopic air holes in glass in most situations, and it is the most favoured optical fibre (Knight et al., 1998). Recently, PCFs have been widely employed in sensing applications due to their reliability in light-analyte interaction depending on the refractive indices of the analytes tested. In terms of sensing applications, PCFs have been utilised in measuring strain, vibration, temperature, chemicals, pressure, torsion, current, displacement, voltage and bending (Mescia and Prudenzano, 2013). Compared to the conventional optical fibres, it benefits in possessing better light confinement, versatility in terms of their birefringence and dispersion, precise sensing, and the implementation of a single-mode for light propagation (Vishwakarma et al., 2017). Generally, the background material of PCFs is manufactured of glass, which ranges from pure silica, BK7, Zeonex, and many

more. There are many types of core designs implemented nowadays; however, the primary core designs are solid-core PCFs and hollow-core PCFs (De et al., 2019). Both structures can be applied depending on the requirements and nature of the experiment. Henceforth, multiple advancements have been researched and integrated into photonic crystal fibres.

A group of researchers (Asaduzzaman et al., 2015) investigated an alcohol PCF sensor of elaborative design that includes 3 rings cladding air holes of circular dimension and 11 core holes arranged hexagonally to detect ethanol and propanol. While the fibre exhibits a complex structure, the sensor only yields a low relative sensitivity of 25.03% but a low confinement loss of about 10^{-12} dB/m, obtained at 0.8 μm operating wavelength. Next, a Surface Plasmon Resonance (SPR)-based photonic sensor was introduced by Ahmed et al. (2019) to detect various alcohols, primarily propanol, butanol, and pentanol. The SPR alcohol sensor depicts relative sensitivities of 41.29% for propanol, 41.30% for butanol, and 41.32% for pentanol, at the wavelength of 1.5 μm, and no confinement losses have been recorded. Such low relative sensitivity was determined by a sensor design of 17 hollow holes arranged in an 'X' pattern and an analyte infiltrated ring situated at the exterior of the cladding, which is considered difficult to fabricate. Additionally, a
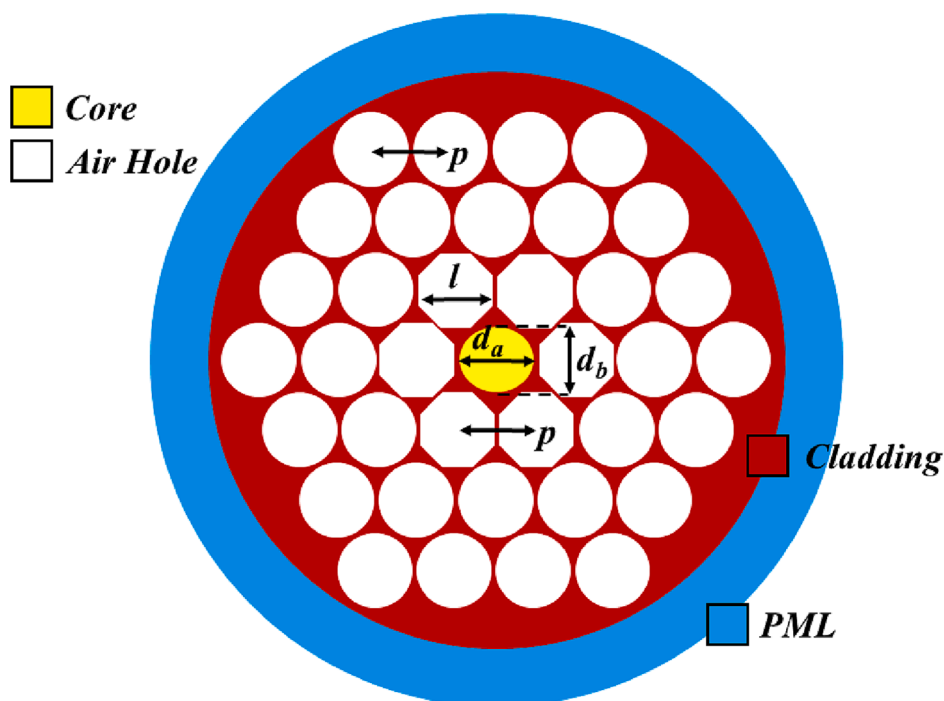
Fig. 1. The architecture of the proposed alcohol sensor.

similar group of researchers (Ahmed et al., 2017) introduced 2 different fibre core designs for alcohol sensing for the selective analyte: propanol, butanol, and pentanol. The initial core design comprises 19 elliptical hollow holes for analyte infiltration that, at 1.5 μm operating wavelength, achieved relative sensitivities of 58.17%, 58.74%, and 59.29% for propanol, butanol, and pentanol, respectively, and about 10^{-10} dB/m for confinement losses for the test analytes. On the other hand, the latter design is consisting of 19 circular core holes that depict little bit better relative sensitivities of 65.95% for propanol, 66.35% for butanol, and 66.73% for pentanol, and confinement losses in the order of 10^{-10} dB/m for all the alcohol analytes. This data is obtained at the same optimum wavelength of 1.5 μm. With the consideration of numerous core holes imposed, the production of the PCF structure shall bear fabrication difficulties. Then, Paul et al. (2017) recommended a 5 circular air hole layers arranged octagonally and a core design of 2 circular hollow hole rings as a porous core alcohol sensor for the selective detection of propanol, butanol, and pentanol. The assessed relative sensitivities for such design are 65.44%, 66.02%, and 66.39% for propanol, butanol, and pentanol, respectively, and confinement losses about 10^{-6} dB/m for propanol, 10^{-10} dB/m for butanol, and 10^{-9} dB/m for pentanol. These data are obtained at an optimum wavelength of 0.8 μm. Lastly, different researchers (Habib et al., 2021) assessed high relative sensitivities of 80.74% for propanol and 84.34% for butanol with low confinement losses of about 10^{-10} to 10^{-11} dB/m for both analytes, at 1.1 operating wavelength. The suggested PCF sensor design incorporated 5 layers cladding air hole in a hexagonal lattice and 1 large circular chore hole. On the contrary in the inclusion of 5 cladding rings in these designs, the photonic fibre sensors are prone to fabrication difficulties and may result in variation from the optimal results.

In the previous studies (Asaduzzaman et al., 2015; Ahmed et al., 2019; Ahmed et al., 2017; Paul et al., 2017; Habib et al., 2021), the form, orientation, and arrangement of the fibre design have impacted the performance of optical properties. Thus, this study has administered a straightforward fibre design incorporating a hollow elliptical core hole with 3 cladding rings of octagonal air holes in the innermost layer and followed by 2 circular air holes and evaluated the different optical properties: effective refractive index, birefringence, power fraction, relative sensitivity, confinement loss, effective area, and nonlinear

coefficients. Notably, the assessed results of the proposed microstructure PCF have proven its applicability in alcohol sensing through its high relative sensitivities and low confinement losses at the optimum wavelength.

2. Design

The proposed microstructure of the PCF biosensor is a simple yet effective design that features an elliptical core hole surrounded by three layers of cladding air holes. The elliptical hole, located at the centre of the fibre, allows for selective sensing of propanol, butanol, and pentanol. The cladding air holes, arranged in a hexagonal lattice, consist of inner octagonal air holes in the first layer and circular air holes in the remaining layers, functioning to reduce loss from the core of the fibre by closely arranging and reducing the refractive index of the cladding region. To prevent stray light from reflecting into the cladding region, the Perfectly Matched Layer (PML) is imposed at the outermost structure of the PCF. The PML of the study was set to 10% of the total fibre diameter, which is a widely accepted value in the literature for similar PCF structures (Islam et al., 2019; Ahmed et al., 2017). This decision was also based on a review of literature (Rahaman et al., 2020) that indicates varying the PML does not significantly affect the performance of the PCF sensor. The proposed PCF sensor design for alcohol detection is shown in Fig. 1.

The dimensions of the proposed PCF design have been meticulously selected through optimization techniques to enhance performance, stability, and fabrication compatibility. The pitch distance can be described as the distance of the centre of one cladding air hole to the centre of its adjacent air hole, which was initially set to 5 μm, followed by fixing the desired Air-Filling Fraction (AFF) value of 0.97, ultimately resulting in the derivation of the diameter dimension $d_a = 4.85$ μm. This approach was carefully taken to ensure that the proposed design meets the necessary requirements for its intended application.

The elliptical core hole has a major axis with a diameter $d_a = 4.85$ μm, whereas the minor axis $d_b = 4.3$ μm. As shown in Fig. 1, the cladding region is composed of 37 cladding air holes arranged in 3 layers with a hexagonal lattice that has an octagonal length $l = 4.8$ μm. With that, the distance between one cladding air hole to another becomes more
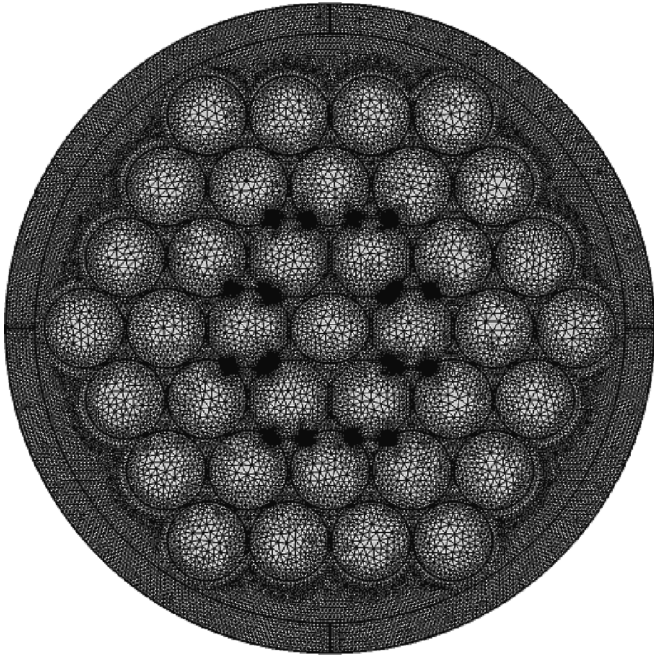
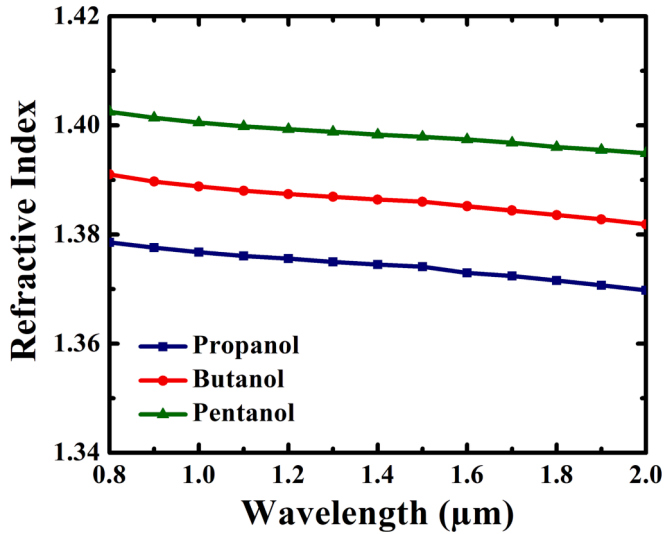**Fig. 2.** Mesh diagram of the proposed PCF sensor for alcohol sensing.

Fig. 3. Refractive indices of propanol, butanol and pentanol against wavelength from 0.8 to 2.0 μm.

packed, which gives rise to better sensing accuracy and lower loss of light.

In consideration of the elaborate manufacturing process involved in fabricating optical fibres, this proposed design is considered simple due to its core design and minimal cladding air holes. Fabrication of this design can be feasibly accomplished using various techniques, including sol–gel (El Hamzaoui et al., 2012), extrusion (Ghazanfari et al., 2017), stack-and-draw (Murphy et al., 2022), and 3D printing (Talataisong et al., 2018). One specific example of the fabrication method for this design is 3D printing, as demonstrated by a previous study (Bertoncini and Liberale, 2020). The specified dimensions of diameter d_a and d_b can be accurately achieved using this method, making it a promising approach for fabricating this type of PCF structure.

3. Methodology

The COMSOL Multiphysics version 5.6 software that is based on the full vector Finite Element Method (FEM) was used to investigate the operation of the proposed microstructure PCF. This approach was used to construct mesh analysis from the derivation of Maxwell's equation, resulting in 28,655 mesh vertices, 56,764 triangular elements, 3,619 edge elements, and 180 vertex elements. Fig. 2 shows the meshing of the proposed PCF design in the mode solver software, applying a fine mesh setting.

Three test analytes were selected: propanol, butanol, and pentanol for the proposed alcohol sensing. For all the alcohol analytes, a set range of operating wavelengths from 0.8 to 2.0 μm was used. With increasing wavelengths, the appropriate refractive indices are shown in Fig. 3 below.

Effective refractive index, birefringence, power fraction, relative sensitivity, confinement loss, effective area, and nonlinear coefficient are the optical parameters to be evaluated to determine the potential and reliability of the proposed microstructure PCF design in practical implementations.

With light interaction between the background material and analyte, the effective refractive index n_{eff} of the fibre structure is defined as (Akowuah et al., 2012):

$$n_{eff}(\lambda) = \sqrt{1 + \frac{A_1\lambda^2}{\lambda^2 - B_1} + \frac{A_2\lambda^2}{\lambda^2 - B_2} + \frac{A_3\lambda^2}{\lambda^2 - B_3}} \qquad (1)$$

where λ is the operating wavelength, $B_{(i=1,2,3)}$ and $C_{(i=1,2,3)}$ are coefficients of that material.

Birefringence measures the difference in effective refractive indices of both *x*- and *y*-polarisation of light (Arif et al., 2019; Yakasai et al., 2019; Agbemabiese and Akowuah, 2020):

$$B = \left| n_{eff}^x - n_{eff}^y \right| \qquad (2)$$

Power fraction *F* is the measure of the power transmitting through the core with respect to the total fibre dimension, and is determined by Yakasai et al. (2019), Podder et al. (2018), Maidi et al. (2021):

$$F = \frac{(sample) \int Re\left(E_x H_y - E_y H_x\right)dxdy}{(total) \int Re\left(E_x H_y - E_y H_x\right)dxdy} \times 100 \qquad (3)$$

where E_x, E_y and H_x, H_y are the transverse electric field and magnetic field in the x- and y-plane, respectively.

Relative sensitivity *R* is the sensing capabilities of the waveguide and the quantification of light-analyte interaction, which is defined by Yakasai et al. (2019), Islam et al. (2018), Maidi et al. (2022):

$$R = \frac{n_r}{n_{eff}} \times F \qquad (4)$$

where n_r is the refractive index of the test analytes: propanol, butanol and pentanol.

Confinement loss *L* is the evaluation of the tendency of light escaping from the core region to the surrounding structure. It can be quantified by Bai et al. (2018), Maji and Roy Chaudhuri (2013):

$$L = \frac{40\pi}{\ln(10)\lambda} Im\left[n_{eff}\right] \times 10^6 \qquad (5)$$

where $Im(n_{eff})$ is the imaginary part of the effective mode index.

Effective area A_{eff} represents the cross-sectional area of the PCF in transverse dimensions and is computed by Jia et al. (2018), Yakasai et al. (2019), Kaijage et al. (2013), Begum and Abas (2018), Begum et al. (2009):

$$A_{eff} = \frac{\left(\int_{-\infty}^{\infty} \int_{-\infty}^{\infty} |E|^2 dxdy\right)^2}{\int_{-\infty}^{\infty} \int_{-\infty}^{\infty} |E|^4 dxdy} \qquad (6)$$
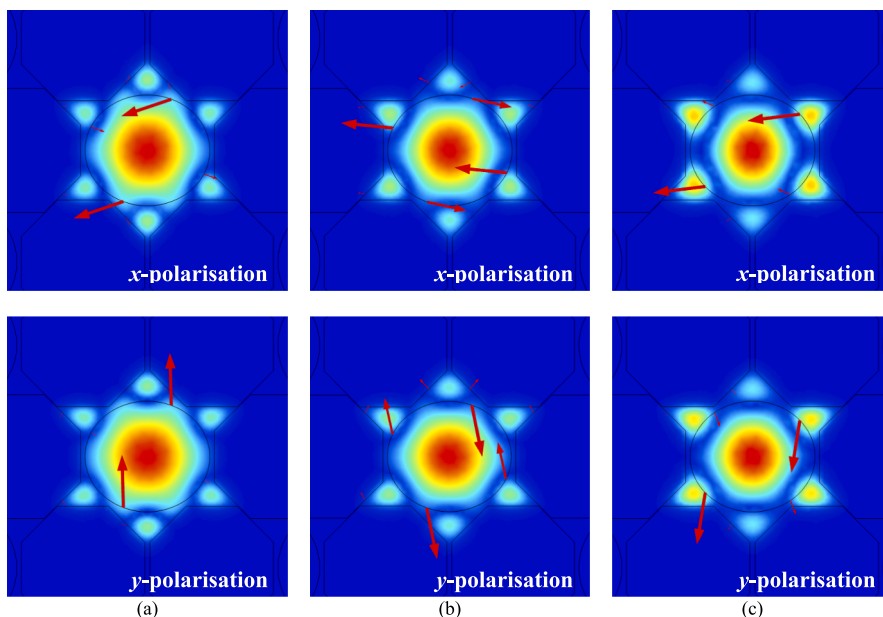
Fig. 4. Mode profile of the proposed PCF alcohol sensor in *x*- and *y*-polarisation for (a) propanol (b) butanol (c) pentanol at 0.8 μm operating wavelength.
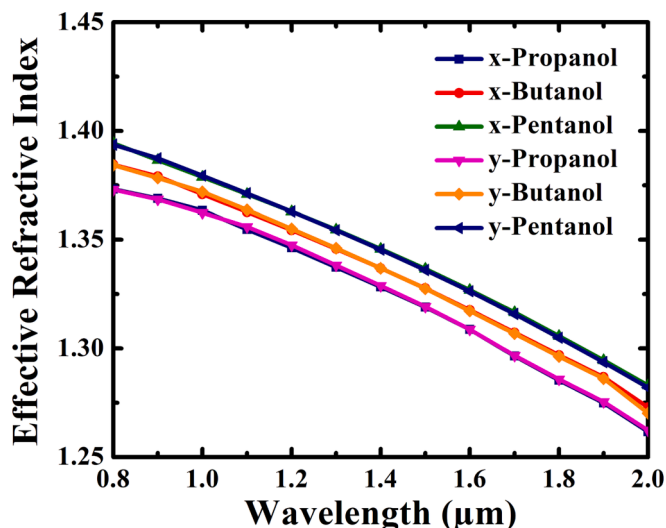

Fig. 5. Results of the effective refractive index of the alcohol test analytes for the proposed microstructure PCF against operating wavelength from 0.8 to 2.0 μm.

Fig. 6. Results of birefringence of the alcohol test analytes for the proposed microstructure PCF against operating wavelength from 0.8 to 2.0 μm.

where E is the transverse electric fields of the guided mode.

The nonlinear coefficient demonstrates the nonlinearity of light interaction with the optical material and is found by Begum and Abas (2018), Kabir et al. (2020), Hossain et al. (2018), Kumar et al. (2020):

$$\gamma = \left(\frac{2\pi}{\lambda}\right)\left(\frac{n_2}{A_{\text{eff}}}\right) \qquad (7)$$

where λ is the operating wavelength and n_2 is the non-linear refractive index.

4. Results and discussion

For each of the analytes, the suggested microstructure PCF sensor was examined to acquire numerical results for optical parameters of effective refractive index, birefringence, power fraction, relative sensitivity, confinement loss, effect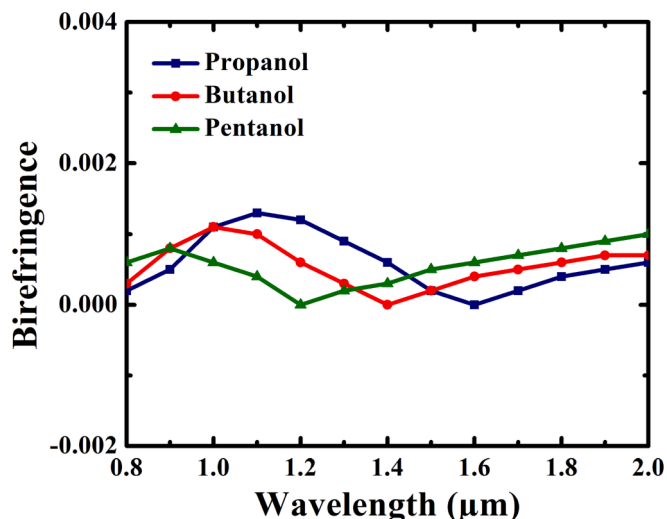ive area, and nonlinear coefficient. The mode profile of the proposed PCF alcohol sensor for propanol, butanol, pentanol at the optimum wavelength is shown in Fig. 4, in both *x*- and *y*-polarisation.

Fig. 5 shows the results of effective refractive index in *x*- and *y*-polarisation of the test analytes in relation to operating wavelength from 0.8 to 2.0 μm. It can be observed that as wavelength rises, the effective refractive indices for all test analytes decrease gradually. In addition, when compared among the selective test analytes, pentanol has the highest effective refractive index than butanol and propanol. This is due to the high refractive index of pentanol, then followed by butanol and propanol. Furthermore, the following optical properties are obtained for *x*-polarisation only, as the effective refractive index difference between *x*- and *y*-polarisation is almost negligible.

The propagation of light within the core of the fibre is dependent on the shape of the core hole, as well as the refractive indices of the background material and test analyte. Due to the asymmetrical dimension of the core hole, light can be directed in different directions, which is known as the polarisation of light. The difference between the axes of
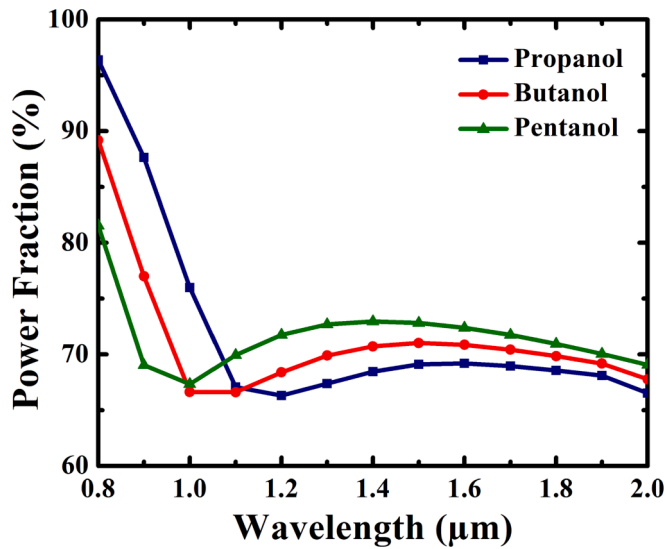
Fig. 7. Results of power fraction of the alcohol test analytes for the proposed microstructure PCF against operating wavelength from 0.8 to 2.0 μm.
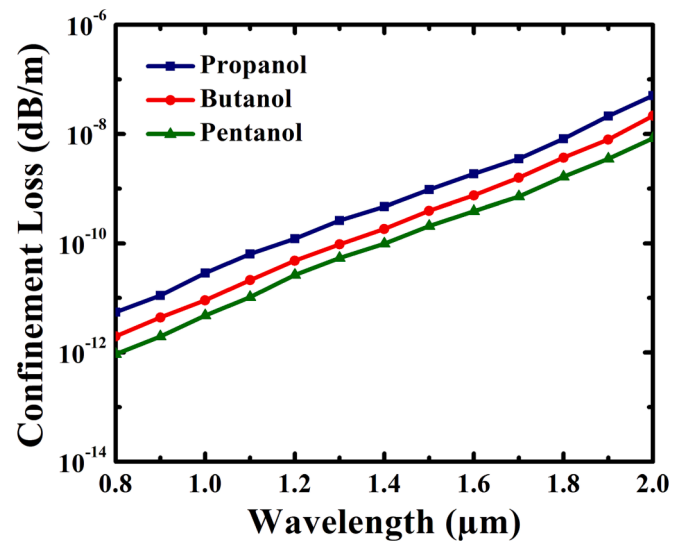

Fig. 9. Results of confinement loss of the alcohol test analytes for the proposed microstructure PCF against operating wavelength from 0.8 to 2.0 μm.
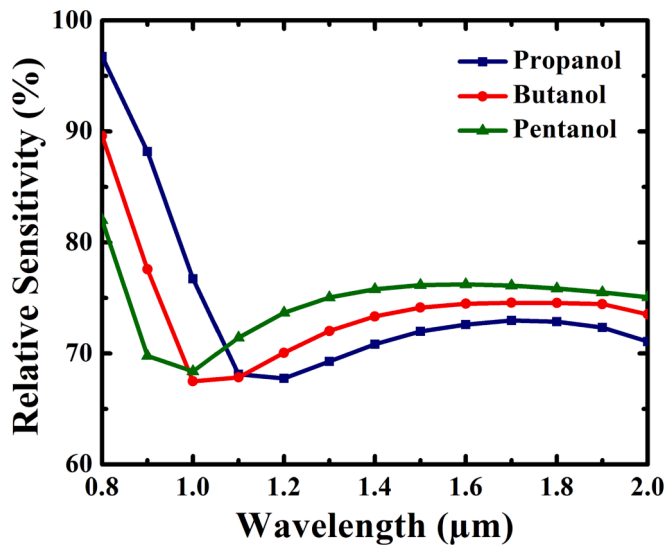

Fig. 8. Results of the relative sensitivity of the alcohol test analytes for the proposed microstructure PCF against operating wavelength from 0.8 to 2.0 μm.
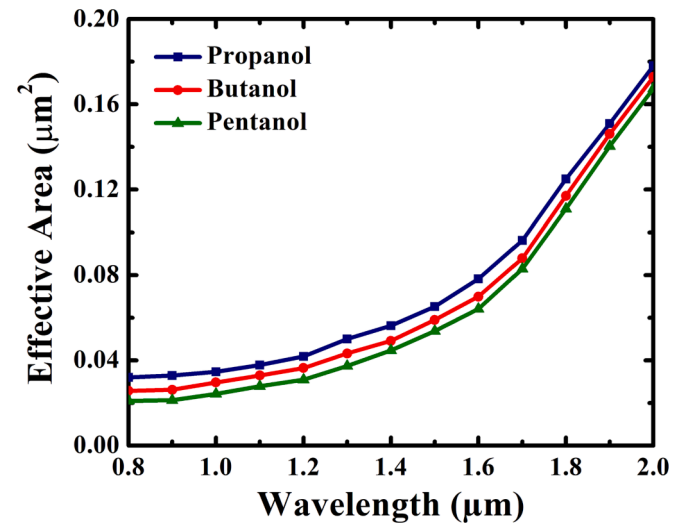

Fig. 10. Results of effective area of the alcohol test analytes for the proposed microstructure PCF against operating wavelength from 0.8 to 2.0 μm.

light polarisation determines the birefringence of the proposed fibre design. Fig. 6 presents the low results of birefringence for the selective test analytes with respect to the wavelengths. For the respective analyte, a similar trend is observed, the birefringence increases at earlier wavelengths, subsequently decreases, and further increases with the increases in wavelength. As the variation range of the birefringence is very small, between 0.0001 and 0.002, it can be considered that the polarisation of light within the core region is negligible.

Fig. 7 displays the power fraction of the proposed microstructure PCF for propanol, butanol, and pentanol with respect to wavelength. The power fraction for all the 3 analytes decreases drastically at the earlier operating wavelength and subsequently increases slightly at approximately 1.0 μm wavelength, then decreases as the operating wavelength increases further. This outcome inferred that most powers are transmitting at the earlier wavelength and develop into a non-uniform behaviour. As the highest value of power fraction is achieved at 0.8 μm wavelength, it is marked as the optimum operating wavelength. At this wavelength, the depicted power fractions are 96.37%, 89.19%, and

81.54% for propanol, butanol, and pentanol, respectively.

Relative sensitivity depends on effective refractive index and power fraction. Thus, the relative sensitivity result of the proposed microstructure PCF against operating wavelength is presented in Fig. 8. As a similar trend to power fraction, the relative sensitivity decreases initially up to about 1.0 μm and gradually increases then decreases as the wavelength increases from 1.0 to 2.0 μm. The relative sensitivities of propanol, butanol, and pentanol at the 0.8 μm operating wavelength have been recorded to be 96.75%, 89.60%, and 82.02% for propanol, butanol, and pentanol, respectively.

Generally, for the selective test analytes, a portion of the light will progressively leak out of the core hole into the surrounding fibre region. This trend is seen in Fig. 9 which shows the confinement loss of propanol, butanol, and pentanol for the proposed sensor at operating wavelengths from 0.8 to 2.0 μm. The increasing trend of confinement losses of the test analytes arises due to the tendency of light signals to escape the waveguide as wavelength increases. At the wavelength of 0.8 μm, the proposed microstructure PCF deduced confinement losses of 5.49×10^{-12} dB/m for propanol, 1.98×10^{-12} dB/m for butanol, and
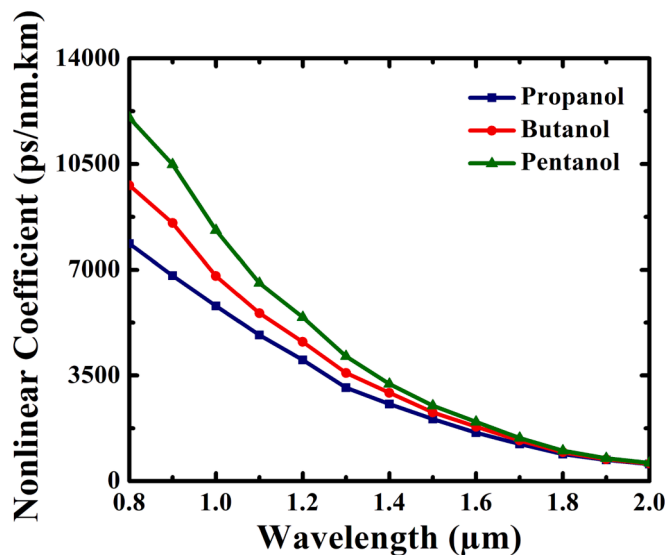
Fig. 11. Results of nonlinear coefficients of the alcohol test analytes for the proposed microstructure PCF against operating wavelength from 0.8 to 2.0 μm.

Table 1
Evaluation table of proposed microstructure PCF against previous studied PCFs at the optimum wavelength.

	Wavelength (μm)	Relative Sensitivity (%)	Confinement Loss (dB/m)
Ref. (Asaduzzaman et al., 2015)	0.8	25.03 (Pr)	$\sim 10^{-12}$ (Pr)
Ref. (Ahmed et al., 2019)	1.5	41.29 (Pr) 41.30 (B) 41.32 (Pe)	–
Ref. (Ahmed et al., 2017)	1.5	58.17 (Pr) 58.74 (B) 59.29 (Pe)	$\sim 10^{-10}$ (Pr) $\sim 10^{-11}$ (B) $\sim 10^{-10}$ (Pe)
Ref. (Ahmed et al., 2017)	1.5	65.95 (Pr) 66.35 (B) 66.73 (Pe)	$\sim 10^{-10}$ (Pr) $\sim 10^{-10}$ (B) $\sim 10^{-11}$ (Pe)
Ref. (Paul et al., 2017)	0.8	65.44 (Pr) 66.02 (B) 66.39 (Pe)	$\sim 10^{-6}$ (Pr) $\sim 10^{-10}$ (B) $\sim 10^{-9}$ (Pe)
Ref. (Habib et al., 2021)	1.1	80.74 (Pr) 84.34 (B)	$\sim 10^{-10}$ (Pr) $\sim 10^{-11}$ (B)
Proposed PCF	0.8	96.75 (Pr) 89.60 (B) 82.02 (Pe)	$\sim 10^{-12}$ (Pr) $\sim 10^{-12}$ (B) $\sim 10^{-13}$ (Pe)

where Pr is propanol, B is butanol, and Pe is pentanol.

9.36×10^{-13} dB/m for pentanol.

Fig. 10 represents the effective area of the proposed fibre with respect to operating wavelength. It can be seen from the graph, the effective area of propanol, butanol, and pentanol increases exponentially with the increases in wavelength. This is due to the phenomenon that the smaller wavelength utilises the small waveguide space while propagating through the core than the higher wavelengths. Propanol, butanol, and pentanol in the proposed microstructure PCF produce effective areas of 0.0320 μm², 0.0257 μm², and 0.0209 μm², respectively, at the optimum wavelength of 0.8 μm.

Fig. 11 shows the graphical illustration of the nonlinear coefficient results against operating wavelength. The nonlinear coefficients of propanol, butanol, and pentanol decrease exponentially as the wavelength increases from 0.8 to 2.0 μm. This trend of the nonlinear coefficient is distinguished due to the opposing nature to the effective area. The nonlinear coefficients of propanol, butanol, and pentanol yield 7857 W⁻¹km⁻¹, 9794 W⁻¹km⁻¹, and 12030 W⁻¹km⁻¹, respectively.

The performance of the proposed sensor is remarkable and suitable for sensing application; thus, Table 1 compares the recorded results to previous studies on PCF alcohol sensors that involves alcohol test analytes. As indicated in Table 1, the proposed PCF design achieved relative sensitivities of 96.75%, 89.60%, and 82.02% for detecting propanol, butanol, and pentanol, respectively, which are higher than those reported in previous studies. Additionally, the confinement loss of the proposed PCF sensor is lower than that of the referenced studies.

Therefore, the proposed PCF sensor has exhibited remarkable sensing performance and is well-suited for sensing applications, outperforming prior PCF sensors in terms of sensitivity and confinement loss.

5. Conclusion

A straightforward microstructure PCF design has been proposed and simulated through the COMSOL Multiphysics software for analyte sensing evaluation. The background material is defined to be fused silica and selective test analytes of propanol, butanol, and pentanol, operating in the lower wavelength range from 0.8 to 2.0 μm. Based on the regular structure of a single elliptical core and 3 cladding air hole rings, the proposed microstructure PCF biosensor has determined the best performance for alcohol sensing among previously suggested PCF sensors. At the optimal wavelength of 0.8 μm, the high depicted relative sensitivities result of 96.75% for propanol, 89.60% for butanol, and 82.02%, confinement losses order for 10^{-12} to 10^{-13} dB/m for these analytes, and other assessed optical properties, the fibre architecture is not limited to sensing applications only but also optical communications, imaging and illumination.

Declaration of Competing Interest

The authors declare that they have no known competing financial interests or personal relationships that could have appeared to influence the work reported in this paper.

Data availability

Data will be made available on request.

References

Agbemabiese, P.A., Akowuah, E.K., 2020. Numerical analysis of photonic crystal fiber of ultra-high birefringence and high nonlinearity. Sci. Rep. 10 (1), 21182. https://doi.org/10.1038/s41598-020-77114-x.

Ahmed, K., Chowdhury, S., Paul, B.K., Shadidul Islam, M., Sen, S., Ibadul Islam, M., Asaduzzaman, S., 2017. Ultrahigh birefringence, ultralow material loss porous core single-mode fiber for terahertz wave guidance. Appl. Opt. 56 (12), 3477. https://doi.org/10.1364/AO.56.003477.

Ahmed, K., Paul, B.K., Chowdhury, S., Islam, M.S., Sen, S., Islam, M.I., Asaduzzaman, S., Bahar, A.N., Miah, M.B.A., 2017. Dataset on photonic crystal fiber based chemical sensor. Data Br. 12, 227–233. https://doi.org/10.1016/j.dib.2017.03.048.

Ahmed, K., Haque, M.J., Jabin, M.A., Paul, B.K., Amiri, I.S., Yupapin, P., 2019. Tetra-core surface plasmon resonance based biosensor for alcohol sensing. Phys. B Condens. Matter 570, 48–52. https://doi.org/10.1016/j.physb.2019.05.047.

Akowuah, E.K., Gorman, T., Ademgil, H., Haxha, S., Robinson, G.K., Oliver, J.V., 2012. Numerical analysis of a photonic crystal fiber for biosensing applications. IEEE J. Quantum Electron. 48 (11), 1403–1410. https://doi.org/10.1109/JQE.2012.2213803.

Arif, M.F.H., Hossain, M.M., Islam, N., Khaled, S.M., 2019. A nonlinear photonic crystal fiber for liquid sensing application with high birefringence and low confinement loss. Sens. Bio-Sensing Res. 22, 100252 https://doi.org/10.1016/j.sbsr.2018.100252.

Asaduzzaman, S.; Arif, M. F. H.; Ahmed, K; Dhar, P. Highly sensitive simple structure circular photonic crystal fiber based chemical sensor. In *2015 IEEE International WIE Conference on Electrical and Computer Engineering (WIECON-ECE)*; IEEE, 2015; pp 151–154. https://doi.org/10.1109/WIECON-ECE.2015.7443884.

Bai, X., Chen, H., Yang, H., 2018. Design of a circular photonic crystal fiber with square air-holes for orbital angular momentum modes transmission. Optik (Stuttg) 158, 1266–1274. https://doi.org/10.1016/j.ijleo.2018.01.015.

Begum, F., Abas, P.E., 2018. Near infrared supercontinuum generation in silica based photonic crystal fiber. Prog. Electromagn. Res. C 2019 (89), 149–159. https://doi.org/10.2528/PIERC18100102.

Begum, F., Namihira, Y., Razzak, S.M.A., Kaijage, S.F., Hai, N.H., Miyagi, K., Higa, H., Zou, N., 2009. Flattened chromatic dispersion in square photonic crystal fibers with low confinement losses. Opt. Rev. 16 (2), 54–58. https://doi.org/10.1007/s10043-009-0011-x.

Bertoncini, A., Liberale, C., 2020. 3D printed waveguides based on photonic crystal fiber designs for complex fiber-end photonic devices. Optica 7 (11), 1487. https://doi.org/10.1364/OPTICA.397281.

De, M., Gangopadhyay, T.K., Singh, V.K., 2019. Prospects of photonic crystal fiber as physical sensor: an overview. Sensors 19 (3), 464. https://doi.org/10.3390/s19030464.

El Hamzaoui, H., Ouerdane, Y., Bigot, L., Bouwmans, G., Capoen, B., Boukenter, A., Girard, S., Bouazaoui, M., 2012. Sol-gel derived ionic copper-doped microstructured optical fiber: a potential selective ultraviolet radiation dosimeter. Opt. Express 20 (28), 29751. https://doi.org/10.1364/oe.20.029751.

Ghazanfari, A., Li, W., Leu, M.C., Hilmas, G.E., 2017. A novel freeform extrusion fabrication process for producing solid ceramic components with uniform layered radiation drying. Addit. Manuf. 15, 102–112. https://doi.org/10.1016/j.addma.2017.04.001.

Habib, M.A., Anower, M.S., AlGhamdi, A., Faragallah, O.S., Eid, M.M.A., Rashed, A.N.Z., 2021. Efficient way for detection of alcohols using hollow core photonic crystal fiber sensor. Opt. Rev. 28 (4), 383–392. https://doi.org/10.1007/s10043-021-00672-6.

Hossain, M., Podder, E., Adhikary, A., Al-Mamun, A., 2018. Optimized hexagonal photonic crystal fibre sensor for glucose sensing. Adv. Res. 13 (3), 1–7. https://doi.org/10.9734/AIR/2018/38972.

Islam, M.R., Kabir, M.F., Talha, K.M.A., Islam, M.S., 2019. A novel hollow core terahertz refractometric sensor. Sens. Bio-Sensing Res. 25, 100295 https://doi.org/10.1016/j.sbsr.2019.100295.

Islam, S., Kumar, B., Ahmed, K., 2018. Liquid-infiltrated photonic crystal fiber for sensing purpose: design and analysis. Alexandria Eng. J. 57 (3), 1459–1466. https://doi.org/10.1016/j.aej.2017.03.015.

Jia, C., Jia, H., Wang, N., Chai, J., Xu, X., Lei, Y., Liu, G., Peng, Y., Xie, J., 2018. Theoretical analysis of a 750-nm bandwidth hollow-core ring photonic crystal fiber with a graded structure for transporting 38 orbital angular momentum modes. IEEE Access 6, 20291–20297. https://doi.org/10.1109/ACCESS.2018.2817577.

Kabir, M.A., Hassan, M.M., Hossain, M.N., Paul, B.K., Ahmed, K., 2020. Design and performance evaluation of photonic crystal fibers of supporting orbital angular momentum states in optical transmission. Opt. Commun. 467, 125731 https://doi.org/10.1016/j.optcom.2020.125731.

Kadhum Hisham, H., 2018. Optical fiber sensing technology: basics, classifications and applications. Am. J. Remote Sens. 6 (1), 1. https://doi.org/10.11648/j.ajrs.20180601.11.

Kaijage, S.F., Ouyang, Z., Jin, X., 2013. Porous-core photonic crystal fiber for low loss terahertz wave guiding. IEEE Photonics Technol. Lett. 25 (15), 1454–1457. https://doi.org/10.1109/LPT.2013.2266412.

Knight, J.C., Birks, T.A., Russell, P.S.J., de Sandro, J.P., 1998. Properties of photonic crystal fiber and the effective index model. J. Opt. Soc. Am. A 15 (3), 748. https://doi.org/10.1364/JOSAA.15.000748.

Kumar, P., Fiaboe, K.F., Roy, J.S., 2020. Design of nonlinear photonic crystal fibers with ultra-flattened zero dispersion for supercontinuum generation. ETRI J. 42 (2), 282–291. https://doi.org/10.4218/etrij.2019-0024.

Maidi, A.M., Yakasai, I., Abas, P.E., Nauman, M.M., Apong, R.A., Kaijage, S., Begum, F., 2021. Design and simulation of photonic crystal fiber for liquid sensing. Photonics 8 (1), 16. https://doi.org/10.3390/photonics8010016.

Maidi, A.M., Shamsuddin, N., Wong, W.-R., Kaijage, S., Begum, F., 2022. Characteristics of ultrasensitive hexagonal-cored photonic crystal fiber for hazardous chemical sensing. Photonics 9 (1), 38. https://doi.org/10.3390/photonics9010038.

Maji, P.S., Roy Chaudhuri, P., 2013. Circular photonic crystal fibers: numerical analysis of chromatic dispersion and losses. ISRN Opt. 2013, 1–9. https://doi.org/10.1155/2013/986924.

Mescia, L., Prudenzano, F., 2013. Advances on optical fiber sensors. Fibers 2 (1), 1–23. https://doi.org/10.3390/fib2010001.

Murphy, L. R.; Yerolatsitis, S.; Birks, T. A.; Stone, J. M. 2022. Stack, seal, evacuate, draw: A method for drawing hollow-core fiber stacks under positive and negative pressure. *Opt. Express 30* (21), 37303. https://doi.org/10.1364/OE.470599.

Paul, B.K., Islam, M.S., Ahmed, K., Asaduzzaman, S., 2017. Alcohol sensing over O+E+S +C+L+U transmission band based on porous cored octagonal photonic crystal fiber. Photonic Sensors 7 (2), 123–130. https://doi.org/10.1007/s13320-017-0376-6.

Podder, E., Jibon, R.H., Hossain, M.B., Al-Mamun Bulbul, A., Biswas, S., Kabir, M.A., 2018. Alcohol sensing through photonic crystal fiber at different temperature. Opt. Photonics J. 08 (10), 309–316. https://doi.org/10.4236/opj.2018.810026.

Rahaman, M.E., Mondal, H.S., Hossain, M.B., Hossain, M.M., Ahsan, M.S., Saha, R., 2020. Simulation of a highly birefringent photonic crystal fiber in terahertz frequency region. SN Appl. Sci. 2 (8), 1435. https://doi.org/10.1007/s42452-020-03210-2.

Talataisong, W., Ismaeel, R., Sandoghchi, S.R., Rutirawut, T., Topley, G., Beresna, M., Brambilla, G., 2018. Novel method for manufacturing optical fiber: extrusion and drawing of microstructured polymer optical fibers from a 3D printer. Opt. Express 26 (24), 32007. https://doi.org/10.1364/OE.26.032007.

Vishwakarma, R.; Kumar, P.; Saha, S.; Rout, G.; Roy, J. S. Zero dispersion photonic crystal fibers for nonlinear applications. In: *2017 8th International Conference on Computing, Communication and Networking Technologies (ICCCNT)*; IEEE, 2017; pp 1–4. https://doi.org/10.1109/ICCCNT.2017.8203910.

Yakasai, I., Abas, P.E., Kaijage, S.F., Caesarendra, W., Begum, F., 2019. Proposal for a quad-elliptical photonic crystal fiber for terahertz wave guidance and sensing chemical warfare liquids. Photonics 6 (3). https://doi.org/10.3390/photonics6030078.

Yakasai, I.K., Abas, P.E., Ali, S., Begum, F., 2019. Modelling and simulation of a porous core photonic crystal fibre for terahertz wave propagation. Opt. Quantum Electron. 51 (4) https://doi.org/10.1007/s11082-019-1832-x.

Yang, J., Ghimire, I., Wu, P.C., Gurung, S., Arndt, C., Tsai, D.P., Lee, H.W.H., 2019. Photonic crystal fiber metalens. Nanophotonics 8 (3), 443–449. https://doi.org/10.1515/nanoph-2018-0204.